Geophysical Journal International

Geophys. J. Int. (2013) doi: 10.1093/gji/ggt133

Geophysical Journal International Advance Access published April 30, 2013

Evidence of upper-mantle processes related to continental rifting versus oceanic crust in the Gulf of California

Xyoli Pérez-Campos[1,2] and Robert W. Clayton[2]

[1]*Departamento de Sismología, Instituto de Geofísica, Universidad Nacional Autónoma de México, Ciudad Universitaria, Coyoacán, Mexico D. F.* 04510, *Mexico. E-mail: xyoli@geofisica.unam.mx*

[2]*Seismological Laboratory, California Institute of Technology, Pasadena, CA* 91125, *USA*

Accepted 2013 April 4. Received 2013 April 3; in original form 2012 June 27

SUMMARY

Receiver functions from teleseismic events, recorded by stations around the Gulf of California, are used to map the upper-mantle seismic discontinuities. We observe a mean transition zone thickness comparable to the global average for most of the region. A low-velocity layer is detected above the 410 discontinuity that varies in thickness along the Gulf of California. The 660 discontinuity shows complex waveforms south of latitude 30°N as a result of the phase change of garnet to perovskite. Within the transition zone, a complex behaviour of the receiver functions is observed mainly at the southern end of the Gulf. The north–south variations of this zone are likely associated with a slab window at the northern Gulf, resulting from the cessation of subduction of the Farallon plate 12 Ma, and the subduction of the Guadalupe and Magdalena microplates at the southern end, resulting in a hydrated upper mantle. Our results suggest that change in rifting styles occurring along the Gulf of California mirrors deeper processes in the upper mantle.

Key words: Mantle processes; Phase transitions; North America.

1 INTRODUCTION

The upper mantle is characterized by two globally observed seismic discontinuities at 410 and 660 km depth (Kennett 1991), which we refer to as the 410 and the 660. They are a sharp velocity change due to olivine phase changes (Ringwood 1970; Jackson 1983). Olivine (α) is transformed to wadsleyite (β spinel) at 410 km depth, and then ringwoodite (γ spinel) turns into perovskite + magnesiowüstite at 660 km depth (Ringwood 1970). From the Clapeyron slopes of these phase transformations, anticorrelated effects on the depth at which they occur are expected in response to lateral temperature variations within the transition zone (TZ) between the 410 and 660 discontinuities. These variations modify the TZ thickness (Bina & Helffrich 1994). A thick TZ may indicate cooler temperatures as would be expected with a subducted slab (Ito & Takahasi 1989; Stammler *et al.* 1992), and a thin TZ may indicate upwelling hot material (Stammler *et al.* 1992; Zhao *et al.* 1997). Also, changes in depth and complexity of the seismic signature of these discontinuities could be due to compositional (e.g. Shearer 1990) or water content variations (e.g. Smyth & Frost 2002; van der Mijde *et al.* 2003; Litasov *et al.* 2005). Hence, the mantle TZ thickness is potentially an indicator of compositional versus thermal effects (Yuen *et al.* 1994).

There is another discontinuity within the TZ, at 520 km depth. This transition is due to the transition from waldsleyite (β spinel) to ringwoodite (γ spinel; Agee 1998). However, this discontinuity is not ubiquitously observed and olivine content variations (Gu *et al.* 1998), iron content variations (Sinogeikin *et al.* 2003) or hydration variations (Inoue *et al.* 1998) are possible explanations for its presence or absence and its simplicity or complexity.

A low-velocity layer (LVL) has been observed immediately above the 410 discontinuity in different regions (e.g. Fee & Dueker 2004; Song *et al.* 2004; Vinnik & Farra 2007; Eagar *et al.* 2010; Jasbinsek *et al.* 2010; Schmandt *et al.* 2011). This layer has been interpreted as a compositional anomaly due to the presence of a dense partial melt. This partial melt has been suggested to be the result of percolation of volatile-rich fluids (Ravenaugh & Sipkin 1994); or of dehydration melting due to the high content of water in the TZ (Bercovici & Karato 2003; Song *et al.* 2004).

Even though olivine is the major mantle component, garnet is also present and it undergoes two phase transitions. The first one (garnet–ilmenite) takes place before 660 km depth, and the second one (garnet–perovskite), occurs around 720 km depth (Vacher *et al.* 1998). Although subtle, this transition results in a velocity change, and given its proximity to the 660, it is possible to observe multiple discontinuities around these depths in some localized regions around the world (e.g. Simmons & Gurrola 2000; Ai *et al.* 2003; Deuss *et al.* 2006). This multiplicity has also been explained as the result of multipathing effects produced by the topography (Lebedev *et al.* 2002).

Receiver function (RF) techniques have proven useful in detecting mantle discontinuities with converted phases. The goal here is to determine the temperature and compositional variations and to relate these to the process of subduction and rifting that have occurred in the Gulf of California (GofC) region.

Until 30 Ma, Farallon Plate was subducting beneath North American. As the ridge approached the trench, the Farallon Plate started breaking into smaller plates (Menard 1978) such as the Guadalupe and Magdalena microplates that subducted under Baja California Peninsula until 12 Ma (Mammericks & Klitgord 1982; Lonsdale 1991; Michaud *et al.* 2006). When the microplate subduction ceased, rifting and extension led to the formation of the present day GofC, which is currently characterized by diffuse continental deformation in the north (Nagy & Stock 2000; Oskin & Stock 2003; González-Fernández *et al.* 2005) and oceanic spreading centres and transform faulting in the south (Lonsdale 1989; Lizarralde *et al.* 2007). This difference has not yet been fully explained, but it may be due to the location of the Farallon slab remnant (Zhang *et al.* 2009), or possibly due to sediments deposited in the northern Gulf by the Colorado River that may have 'drowned' the normal ocean ridge process (González-Fernández *et al.* 2005).

In this paper, we present an analysis of the mantle TZ to determine if it has similar lateral variations as the rifting process. If it does, it will favour the remnant-slab explanation of the rift variations. Otherwise, it will indicate that it is due to a relatively shallow process, such as the sedimentation.

2 DATA

From 2002 April to 2007 April, the Network of Autonomously Recording Seismographs (NARS)-Baja network operated in Baja California and Sonora, Mexico (Clayton *et al.* 2004) with 12 stations along the peninsula of Baja California and four stations on the continental side. This network was complemented with five stations, distributed around the Gulf, from the Red Sísmica de Banda Ancha (RESBAN) of Centro de Investigación Científica y de Educación Superior de Ensenada (Cicese). Since 2006, the Servicio Sismológico Nacional (SSN) has been expanding its network, installing stations in northern Mexico, with nine of them around the GofC. These 30 stations give us good coverage for the GofC region, including both the peninsula and the continental side. The distribution of the stations is shown in Fig. 1. We selected teleseismic events with M_w above 5.8 in a distance range between 30° and 90° (Fig. 2a) and with an identifiable *P*-wave arrival that were recorded during the period of operation of each station. In all, we obtain 1723 RFs, and the number of RFs per station is shown in Fig. 2(b). We have also added data from 16 stations of the Southern California Seismic Network (SCSN) to extend our coverage to the North. However, to maintain an even distribution of RFs in the Gulf region (our main focus), we excluded them from the main body of the paper. The results using also the SCSN stations are included as part of the Supporting Information.

3 ANALYSIS OF THE CONVERTED PHASES

We employed the RF technique (Vinnik 1977), with a 120 s data window, starting 30 s before the *P*-wave onset. The three components of the seismogram, *Z*-vertical, *N*-North, *E*-East, are first rotated to a Z-vertical, *R*-radial and *T*-transversal system. We performed an extra rotation to a *P*-polarization coordinate system with components *L* in the ray direction, *Q* and *T* in the radial and transverse components, respectively. The last rotation is done by finding the eigenvectors of the covariance matrix and maximizing, with the rotation, the *P* energy on the *L* component (Kanasewich 1973; Husebye *et al.* 1975; Vinnik 1977). We deconvolve the *Q* component by the *L* component

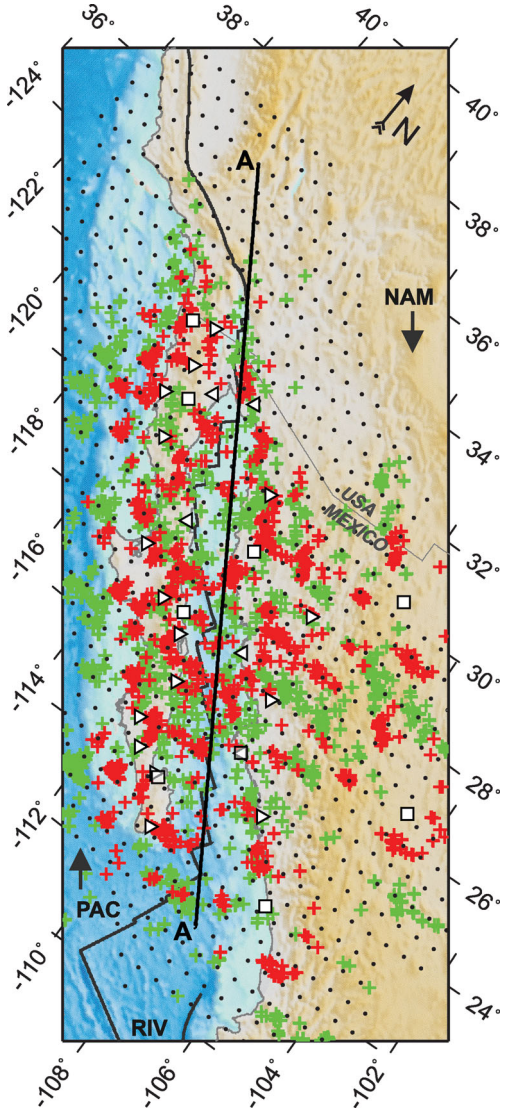

Figure 1. Station locations and pierce points for the 410 (red crosses) and the 660 (green crosses) discontinuities. Right triangles denote NARS-Baja stations; left triangles, RESBAN stations; and squares, SSN stations. The black dots correspond to the 0.5° × 0.5° grid nodes. Profile AA′ is shown in Fig. 5. Thick black arrows indicate the current Pacific (PAC)–North America (NAM) relative plate motion direction N37°W (Atwater & Stock 1998). RIV, Rivera Plate.

in the time domain (Ligorría & Ammon 1999), filtering out the high frequencies with a Gaussian filter with a width parameter of 2.5. We chose the RFs that when convolved with the *L* component reproduce at least 70 per cent of the *Q* component. In order to enhance the mantle discontinuity arrivals, we further filtered the resulting RFs between 0.025 and 0.3 Hz (Fig. 2c).

Following Dueker & Sheehan (1997), we stacked the RFs according to their common conversion points. We used both iasp91 (Kennett & Engdahl 1991) and TNA (Grand & Helmberger 1984) as reference velocity models to back-project the RFs along their ray paths and identify their conversion points at the 410 and the 660 (Fig. 1). Since the TNA model is only shear wave velocities, we used the same V_P/V_S as for iasp91. We only present the results for iasp91 model since the observed arrival times of phases $P_{410}s$ and $P_{660}s$ agree better with the theoretical arrivals for iasp91 model than for TNA model. Results for TNA model are shown in the Supporting

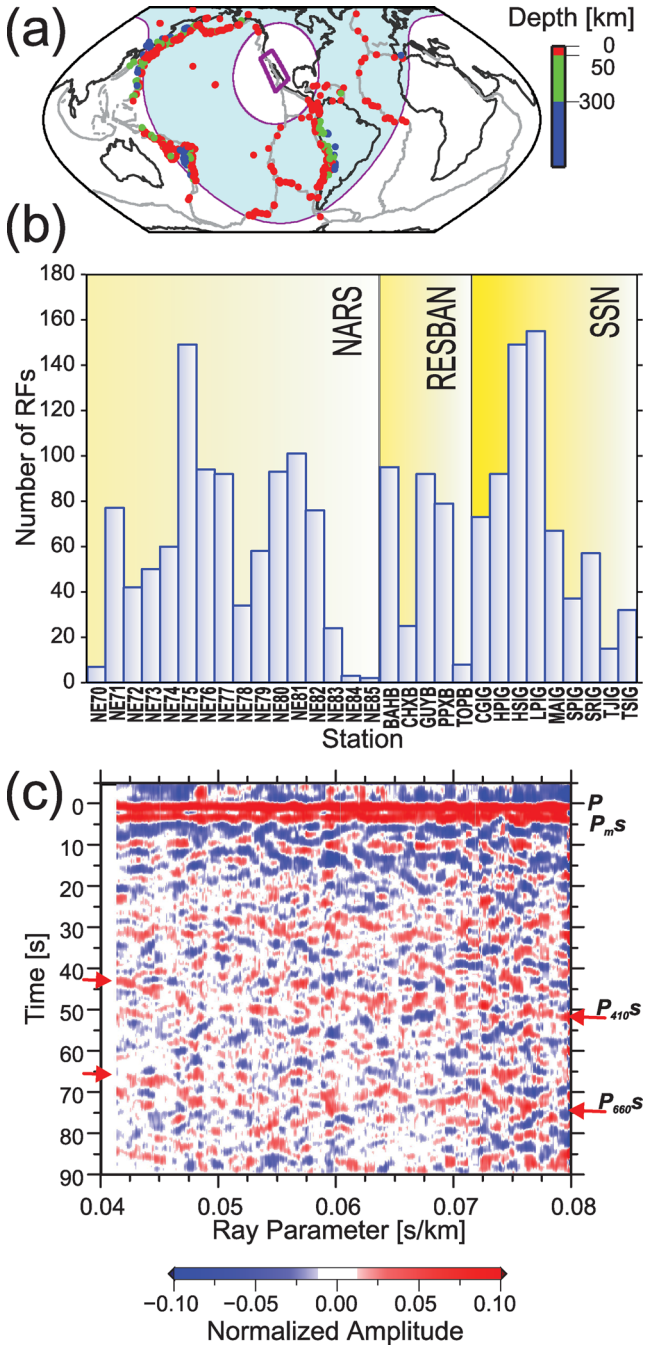

Figure 2. Events and RFs. (a) Location of the selected events, colour coded by depth. The rectangle comprises the area in Fig. 1; the shaded region denotes a distance range of 30°–90° from the centre of the rectangle. (b) Number of RFs obtained at each station. The stations are grouped by network. (c) Receiver functions stacked by ray parameter. The RFs have been filtered between 0.025 and 0.3 Hz. The direct *P* arrival (*P*) is aligned at zero. The conversion from the Moho ($P_m s$) arrives before 5 s. The theoretical arrivals for the 410 ($P_{410}s$) and the 660 ($P_{660}s$) are denoted by red arrows. For the 410, a positive pulse is consistently later than the theoretical arrival of the iasp91 model suggesting that the 410 is depressed with respect to the iasp91 discontinuity in all the study area.

Information for completeness. Previous studies have shown that using a 1-D model versus a 3-D model led to only small differences in the upper-mantle discontinuities (e.g. Owens *et al.* 2000) and depth uncertainties of ±5 km (e.g. Gurrola & Minster 1998; Owens *et al.* 2000), and hence we use only 1-D reference models in this study. We note that the variation in shear velocities in the upper mantle observed by Wang *et al.* (2009, Fig. 1) do not correlate with the thickness changes in the TZ estimated here.

Based on Gilbert *et al.* (2003), we generated a 0.5° × 0.5° grid (Fig. 1) and stacked the RFs within a distance of 1.5°, for each discontinuity. The number of RFs at each node is shown in Fig. 3(a). The minimum number of RFs allowed in each node in order to perform the stacking is 10. In the Gulf region, there are at least 50 RFs per node. With the stacking, we obtained the mean RF and its confidence interval at each node by bootstrapping the RFs at each node (Efron & Tibshirani 1993).

4 TOPOGRAPHY OF THE DISCONTINUITIES

The topography obtained for each discontinuity is shown in Fig. 3. An automatic picker was first employed to delineate the topography; however, given the complexity of the RFs, it was followed by a visual inspection and a manual adjustment to ensure the picks were following laterally coherent phases. In order to verify the observed features, we performed a random test by bootstrapping all the RFs and stacking the same number of RFs as in the original result at each node (*cf.* Gilbert *et al.* 2003). The difference between the topography derived from the cumulative data set and the randomly resampled data set shows random patterns with no apparent structure (Fig. 3c). Results using TNA model are shown in Fig. S2.

To assess the complexity of the RFs, we identify the number of peaks and valleys (NPV) for the mean RF at each node. NPV is defined as the number of maxima and minima that exceed 80 per cent of the maximum value observed in the RF (Fig. 3b), as long as it has a zero crossing in between (Fig. 3f). We tried other values for the percentage level (between 70 and 90 per cent) with no significant difference on the results. For the 410, we obtain the NPV from 300 to 460 km depth, while for the 660, the range between 610 and 800 km depth is used. An NPV between 1 and 3 represents a single pulse in the RF, suggesting a simple discontinuity. A value of 4 or larger suggests a complex discontinuity, such as a possible LVL on top of the 410 discontinuity or multiple phase conversion in the case of the 660 discontinuity.

No time correction was applied to the RFs, thus our interpretation is in the frame of the reference model. The 410 is depressed in the entire region by 19 ± 7 km on average with respect to the 410 of iasp91 model, and consequently we show in Fig. 3(d) the topography with respect to a constant depth of 429 km. This depth is consistent with that predicted for the 410 by the velocity model of Wang *et al.* (2009). In the middle of the Gulf, there is a small hill between 27°N and 30°N, marked with a 'T' in Fig. 3, where the 410 is found at shallower depths than its surroundings. This coincides with a region where the RFs appear simpler, and on the surface, it correlates to the transition from continental rifting in the north of the Gulf to oceanic crust in the south.

The 660 is also depressed with respect to iasp91 by 10 ± 13 km, with the deepest region between 27°N and 30°N on the east side of the Gulf (Fig. 3d). In general, the RFs for the 660 discontinuity are simpler except south of 28°N within the Gulf and to the east of it.

The thickness of the TZ has an average of 243 ± 14 km, which is close to that of iasp91 (250 km). It shows thinner regions in northern Baja California (225 ± 7 km) and the southern end of the Gulf (238 ± 4 km), and thicker regions (260 ± 7 km) between 27°N and 30°N (Fig. 4b).

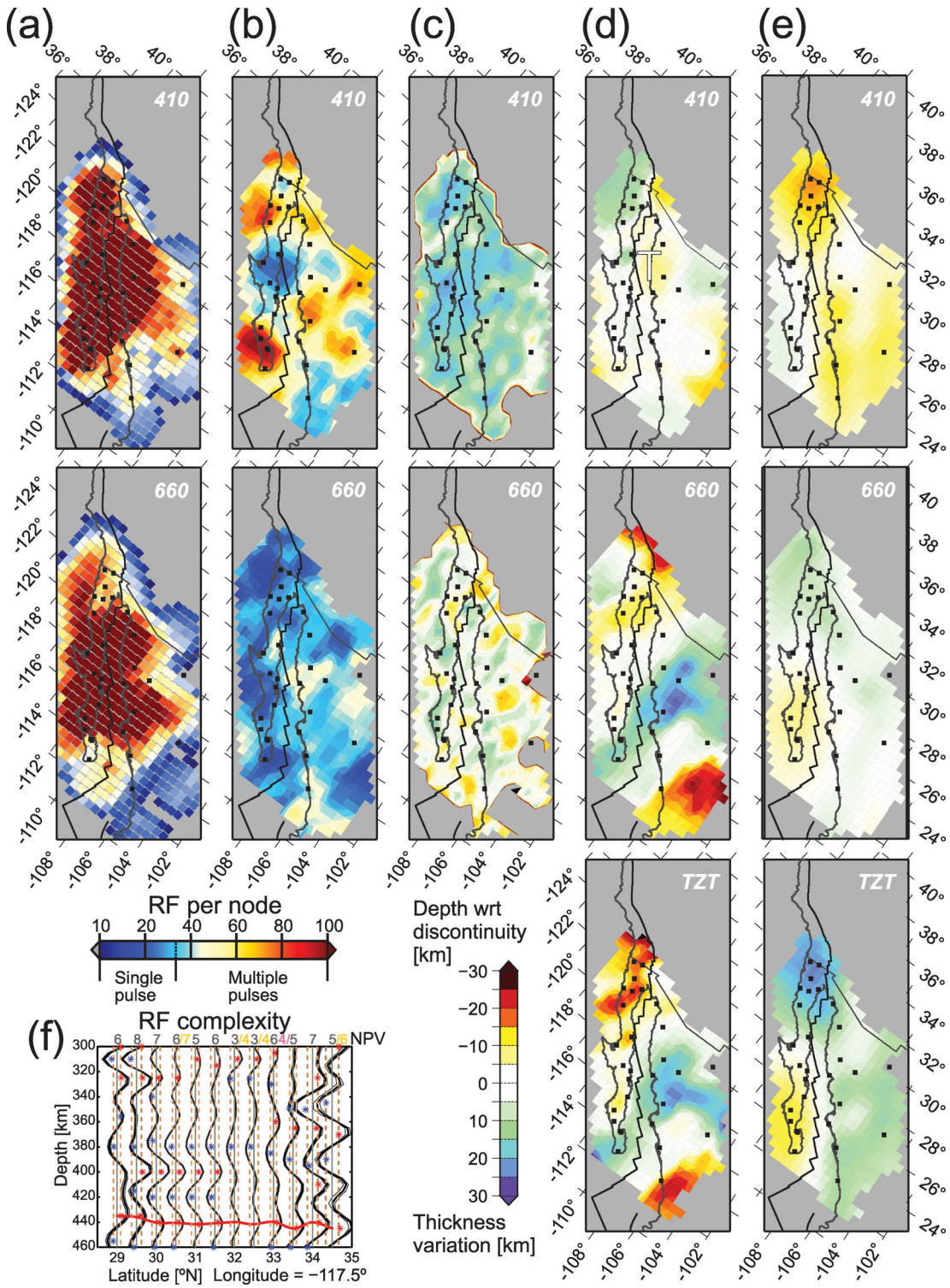

Figure 3. Upper-mantle discontinuities and transition zone thickness. (a) Number of RFs per node for the 410 (top) and the 660 (bottom). The minimum allowed for the stacking was 10. (b) Complexity of the RFs for the 410 (top) and the 660 (bottom). The colour corresponds to the NPV for the mean RF at each node, blue colours denote a single pulse, while warm colours denote multiple pulses. (c) Topography of the 410 (top) and 660 (bottom) from the bootstrap test described in the text. (d) Topography of the 410 (top) and 660 (centre). The colour corresponds to the depth with respect to 429 km average depth for the 410 and 670 km for the 660. 'T' denotes a hill in the 410, described on the text. The bottom panel shows the transition zone thickness (TZT), colour corresponds to the variation with respect to the average of 243 km. (e) Topography obtained from the global tomography by Li *et al.* (2008), for the 410 on the top panel and for the 660 on the bottom as described on the text, following Fukao *et al.* (2009). The bottom panel shows the difference between them as a proxy for the TZT. (f) Example of the NPV estimation, the vertical dashed lines denote the 70 per cent (in yellow), 80 per cent (in grey) and 90 per cent (in pink) of the maximum value of the RF (in black thick line). Confidence intervals for the RFs are shown as thin grey lines, but are not always obvious because the interval is too narrow to be evident in this scale. Stars in red denote a peak and in blue a valley. The numbers in grey on the top are the NPV for each RF, in yellow for the 70 per cent level and in pink for the 90 per cent level, in case it differs from the value obtained at 80 per cent level.

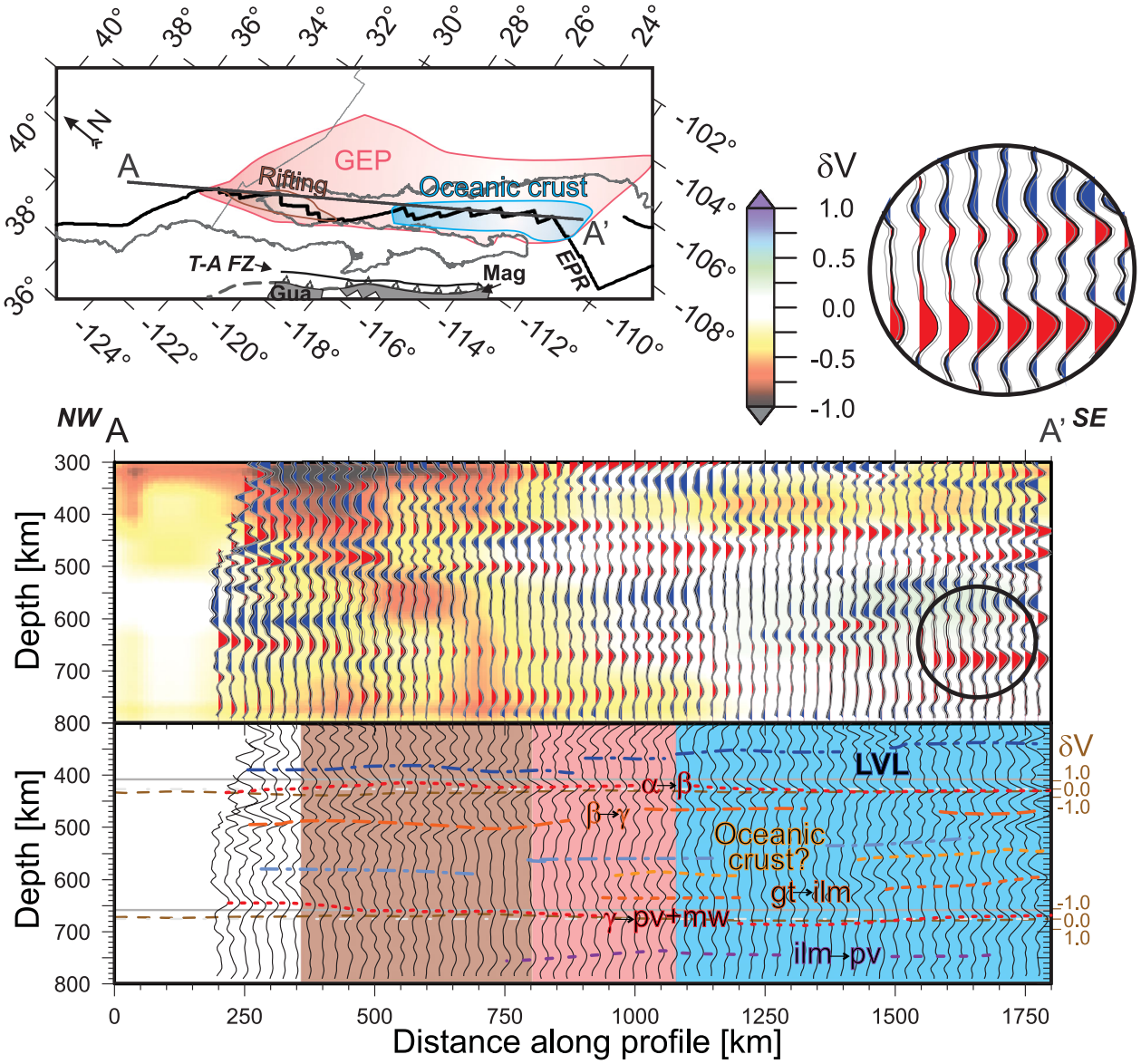

Figure 4. Profile along the Gulf of California. Top: Surface provinces in the region of the study and location of profile AA′. The grey areas correspond to the remains of the Guadalupe (Gua) and Magdalena (Mag) plates. T-A FZ, Tosco-Abreajos fault zone; EPR, East Pacific Rise; GEP, Gulf Extension Province. Centre: RFs within 50 km from profile AA′, superimposed to the tomography from Li *et al.* (2008). The colour board denotes the *P*-wave percentage perturbation. Bottom: Interpretation of profile A–A′; background colours denote the region: brown for continental rifting, blue for oceanic crust and pink for the transition. Red, orange and magenta dashed lines denote positive phases; light and dark blue, negative phases. The brown dashed lines denote the 410 and 660 estimated from the tomography model by Li *et al.* (2008). Continuous grey lines denote depths of 410 and 660 km; the dashed-dotted grey lines denote the average depth for the 410 and 660 obtained from RFs. gt, garnet; ilm, ilmenita; pv, perovskite; mw, magnesiowüstite. The inset shows a blow-up of a subset of RFs and their confidence intervals.

We compare the topography obtained from our RF analysis with that estimated from the tomography by Li *et al.* (2008). For the comparison, we convert the tomographic features to relative depth changes of the discontinuities (Fig. 3e). To translate the velocity anomaly to depth, we use a factor of −16 km/per cent that corresponds to a Clapeyron slope of 3.0 MPa K^{-1} for the 410; that is, that for 1 per cent velocity change observed on the tomography, the 410 will be shifted shallower by 16 km. For the 660, we use a factor of 20 km/per cent from a Clapeyron slope of −2.5 MPa K^{-1} (see Fukao *et al.* 2009).

Comparing with the tomographic models of Li *et al.* (2008), the 410 delineated by the RFs is depressed, except for the region in the central Gulf, between 27° and 30°. The 660 is found shallower than the surrounding, as a hill, in the northern Gulf and it is found deeper, as a valley, on the southern Gulf, the rest of the region shows no significant topography. The TZ thickness translates into a thin zone north of 29° and a thick zone to the south.

It is clear that there is a change in the TZ along the Gulf. We further analyse this in a profile along the Gulf axis. Fig. 4 shows the stacked RFs within a 50 km distance from the profile, superimposed on the global tomography by Li *et al.* (2008). The arrivals for the 410 and the 660 are identifiable along the profile, and the complexity of the RFs at the southern end is evident. Besides the 410 and the 660 discontinuities, the stacked RFs show an emergent positive pulse at ∼500 km depth and a negative pulse between 550 and 600 km depth at the north of the profile (Fig. 4). The TZ is more complicated

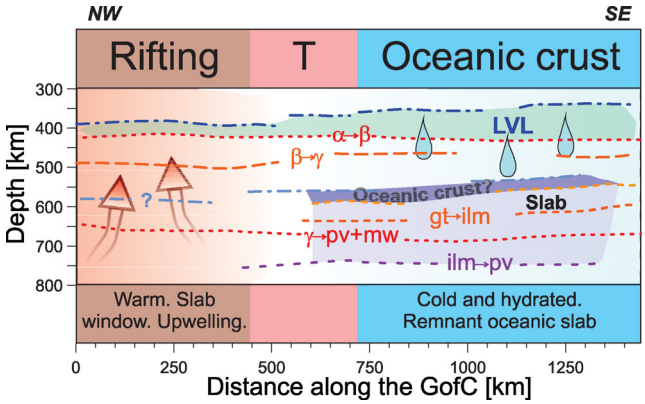

Figure 5. Mantle transition zone along the Gulf of California. Top: Rifting styles. T, transition. Bottom: Observation and interpretation as in Table 1. Blue drops indicate hydrated TZ as a result of dehydration from the slab. Arrows indicate upwelling. Red, orange and magenta dashed lines denote positive phases observed in the RFs; light and dark blue, negative phases. gt, garnet; ilm, ilmenita; pv, perovskite; mw, magnesiowüstite.

at the southern end, where several positive and negative pulses are observed between the 410 and 660. From 30° to the south, an extra positive pulse can be traced at ∼750 km depth. This complexity in the RFs is not correlated with the sporadic presence of shallower discontinuities (Supporting Information).

5 DISCUSSION

The 410- and the 660-discontinuity depth might be affected by velocity anomalies above or below them. In our case, both discontinuities seem to be shifted deeper, the 410 by ∼19 km and the 660 by ∼10 km. As observed in other studies (e.g. Lebedev *et al.* 2002), the TZ thickness is not significantly affected by velocity anomalies above the TZ. In our case, the TZ thickness coincides in general terms with the global tomography by Li *et al.* (2008) in the northern Gulf, where the tomography shows slow/hot material, and is ∼30 km thinner than in the south, where the tomography shows fast/cold material. This difference is consistent with a 200 K temperature change between the two regions, assuming a Clapeyron slope of 3.0 MPa K^{-1} for the 410 and −2.5 MPa K^{-1} for the 660. A LVL is observed above the 410 discontinuity along the Gulf that thickens at the southern end. South of 29°N, the RFs show more complexity (Figs 3 and 4). Here, we discard multipathing as the cause of the complexity since the observed topography is smooth and shows gradients of less than a 10 per cent slope.

Following the profile in Fig. 4 from north to south, we can distinguish two main regions that on the surface can be correlated to what we observe in the mantle TZ (Table 1; Fig. 5): continental rifting and generation of oceanic crust, with a transition between them. As will be discussed below, evidence suggests that the first one is characterized by a warm TZ, consistent with upwelling while the second one is characterized by a cold and hydrated TZ (Fig. 5).

5.1 Continental rifting

A negative phase is observed above the 410 discontinuity, indicating a ∼30 km thick LVL. This layer can be the result of a hydrous melt layer created by the TZ water filter (Bercovici & Karato 2003). This hypothesis is favoured among others (e.g. velocity anisotropy anomaly, a subsolidus chemical anomaly) due to the rapid lateral changes observed over short distances (e.g. Eagar *et al.* 2010; Jasbinsek *et al.* 2010). As shown in Fig. 3(c), the 410 is depressed with respect to iasp91 but slightly shallower with respect to the southern end of the Gulf (∼5 km). In Fig. 4, a subtle positive phase can be observed at ∼500 km that might correspond to the transition from waldsleyite to ringwoodite. Below this, at ∼525 km depth, a negative phase can be observed but its explanation is not currently understood. The 660 discontinuity is denoted by a single positive phase (Figs 4 and 5), and at a shallower depth in the north than for the rest of the Gulf by 20–30 km. The TZ is thinner the than global average by ∼20 km. All these observations characterize this region as a warm region, consistent with the global tomography by Li *et al.* (2008).

5.2 Oceanic crust

The LVL doubles its thickness to ∼60 km in the southern end of the Gulf. Within the TZ at least three pulses are clearly identifiable, the first one of which is a positive pulse, at ∼480 km, which is most likely related to the transition from waldsleyite to ringwoodite, shifted to shallower depths due to the presence of cold material (Sinogeikin *et al.* 2003). Also, a negative–positive pair is observed between 500 and 600 km, and as noted by Sinogeikin *et al.* (2003), this might indicate the presence of subducted oceanic crust. Another positive phase is further identified at ∼600 km, this phase might correspond to the transition from garnet to ilmenite (Vacher *et al.* 1998). A double positive phase at depths between 500 and 600 km, has been observed in other regions (e.g. Deuss & Woodhouse 2001), suggesting a difference in both temperature and composition (Deuss & Woodhouse 2001; Sinogeikin *et al.* 2003). Further down, the 660 discontinuity appears as a double positive pulse that separates up to ∼70 km at the southern end of the Gulf. The first pulse would correspond to the transition from ringwoodite to perovskite + magnesiowüstite, while the deeper pulse would correspond to the transition from ilmenite to perovskite (Litasov *et al.* 2005). This complex RF structure is consistent with a cold region due to the presence of a slab and a hydrated TZ.

Along the Baja margin, the Farallon slab was subducting and breaking in to smaller plates. As the ridge approached the trench (∼100 km), subduction stopped and a slab window was generated at the northern end but subduction continued in the south (e.g. McCroy *et al.* 2009). In Southern California, the Monterey and Arguello microplate were subducted and a slab window allowed the upwelling of asthenospheric material. The slab continued its subduction to the east and remnants should be found east of our focus region. In Baja California, the Guadalupe and Magdalena plates stopped subducting before the ridge reached the trench (Burkett & Billen 2010). These plates were trapped by the Pacific Plate (Lonsdale 1991). They might have broken at shallow depths (∼50 km), leaving remnants under the peninsula (Ferrari *et al.* 2002; Persaud *et al.* 2007; Burkett & Billen 2010). According to 3-D modelling (Burkett & Billen 2010), the broken slab would have descended almost vertically into the mantle, so the presence of the slab is expected at the TZ depths south of 27°N. Global tomography by Li *et al.* (2008) shows a slow anomaly to the north and a fast anomaly to the south, consistent with this interpretation and our results from RFs. An interpretation solely based on temperature anomaly is not sufficient to explain the complexities on the RFs and the depth of the 410 and the 660 observed. Therefore, a composition variability and hydration is suggested. The presence of the subducted slab could explain the temperature anomaly, the composition variability and hydration.

Table 1. Summary of the discontinuities behaviour in the Gulf regions.

	Observed phases—Interpretation			
Depth	Rifting of continental crust		Generation of oceanic crust (oceanic floor spreading)	
Above 410 km	Negative phase, ∼30 km thick	LVL	Negative phase, ∼60 km thick	LVL
410 km	Positive phase, at ∼425 km	$\alpha \rightarrow \beta$	Positive phase, at ∼430 km	$\alpha \rightarrow \beta$
Between 450 and 650 km	Positive phase at ∼500 km	$\beta \rightarrow \gamma$	Positive phase at ∼ 480 km	$\beta \rightarrow \gamma$
	Negative phase at ∼575 km	*?*	Pair of negative–positive phases between 500 – 600 km	Oceanic crust
			Positive phase at ∼ 600 km	gt → ilm
660 km	Positive phase at shallower depth than the rest of the gulf.	$\gamma \rightarrow$ pv + mw	Positive phase at ∼690 km	$\gamma \rightarrow$ pv + mw
			Positive phase at ∼750 km	ilm → pv
Interpretation	Warm system Consistent with slab window and upwelling		Cold and hydrated system, the the source of the water might be the remnant oceanic slab	

gt, garnet; ilm, ilmenita; pv, perovskite; mw, magnesiowüstite.

Seismic evidence for water being transported to the TZ in the Tonga region by a subducted slab has been presented by Savage (2012).

Our results then suggest that the change in the rifting process occurring along the GofC mirror deep processes in the upper mantle (Fig. 5). Since the southern Gulf appears to be a hydrous system, this might indicate that the presence of the oceanic slab in the region is the source of the extra water compared with the northern Gulf.

6 CONCLUSIONS

We characterize the mantle TZ by means of RFs. Two regions can be distinguished along the GofC axis based on their RFs and we can interpret them in terms of the presence of the slab. In the north, where continental rifting is occurring, the TZ is characterized as a warm system, consistent with a slab window that allowed upwelling. In the south, where ocean floor spreading (generation of oceanic crust) is occurring, the TZ is characterized as a cold and hydrated system; this seems to be the result of the remnant oceanic slab. The change in rifting style at the surface is evidence of deeper processes, and this study provides a link to the presence of the slab and the slab window.

ACKNOWLEDGEMENTS

Figures were done using Generic Mapping Tools (Wessel & Smith 1991). We thank three anonymous reviewers whose comments improved this paper. We thank Cicese for data and maintenance of the RESBAN and NARS-Baja stations and the SSN and the SCSN for their data and station maintenance. The operation of the RESBAN array (Red Sismológica de Banda Ancha del Golfo de California) has been possible thanks to the financial support of the Mexican National Council for Science and Technology (Conacyt) by means of the projects 48852, 62116. Partial funding for this work was provided by project DGAPA-IN105910, and by the Tectonics Observatory at Caltech, which is funded by the Betty and Gordon Moore Foundation. This is contribution #203 from the Tectonics Observatory. X.P.-C. had a sabbatical fellowship from DGAPA-UNAM and thanks the Tectonics Observatory at Caltech for partial funding.

REFERENCES

Agee, C.B., 1998. Phase transformation and seismic structure in the upper mantle and the transition zone, in *Ultrahigh-Pressure Mineralogy: Physics and Chemistry of the Earth's Deep Interior, Reviews in Mineralogy,* Vol. 37, pp. 165–203, eds Hemley, R.J. & Ribbe, P.H., Mineralogical Society of America, Washington, DC.

Ai, Y., Zheng, T., Xu, W., He, Y. & Dong, D., 2003. A complex 660 km discontinuity beneath northeast China, *Earth planet. Sci. Lett.,* **212,** 63–71.

Atwater, T. & Stock, J., 1998. Pacific-North America plate tectonics of the Neogene southwestern United States: an update, *Int. Geol. Rev.,* **40,** 375–402.

Bercovici, D. & Karato, S.-I., 2003. Whole-mantle convection and the transition-zone water filter, *Nature,* **425,** 39–44.

Bina, C.R. & Helffrich, G., 1994. Phase transition Clapeyron slopes and transition zone seismic discontinuity topography, *J. geophys. Res.,* **99,** 15 853–15 860.

Burkett, E.R. & Billen, M.I., 2010. Three-dimensinality of slab detachment due to ridge-trench collision: laterally simultaneous boudinage versus tear propagation, *Geoche. Geophys. Geosyst.,* **11,** Q11012, doi:10.1029/2010GC003286.

Clayton, R.W. *et al.*, 2004. The NARS-Baja seismic array in the Gulf of California rift zone, *MARGINS Newsl.,* **13,** 1–4.

Deuss, A. & Woodhouse, J., 2001. Seismic observations of splitting of the mid-transition zone discontinuity in Earth's mantle, *Science,* **294,** 354–357.

Deuss, A., Redfern, S.A.T., Chambers, K. & Woodhouse, J.H., 2006. The nature of the 660-kilometer discontinuity in Earth's mantle from global seismic observations of PP precursors, *Science,* **311,** 198–201.

Dueker, K.G. & Sheehan, A.F., 1997. Mantle discontinuity structure from midpoint stacks of converted P to S waves across the Yellowstone hotspot track, *J. geophys. Res.,* **102,** 8313–8327.

Eagar, K.C., Fouch, M.J. & James, D.E., 2010. Receiver function imaging of upper mantle complexity beneath the Pacific Northwest, United States, *Earth planet. Sci. Lett.,* **297,** 140–152.

Efron, B. & Tibshirani, R.J., 1993. *An Introduction to the Bootstrap, Monographs on Statistics and Applied Probability,* Vol. 57, p. 436, Chapman & Hall/CRC, Boca Raton, FL.

Fee, D. & Dueker, K., 2004. Mantle discontinuity structure from midpoint stacks of converted P and S waves across the Yellowstone hotspot track, *J. geophys. Res.,* **102**(B4), 8313–8327.

Ferrari, L., López-Martínez, M. & Rosas-Elguera, J., 2002. Ignimbrite flare-up and deformation in the southern Sierra Madre Occidental, western Mexico: implications for the late subduction history of the Farallon plate, *Tectonics,* **21,** doi:10.1029/2001TC001302.

Fukao, Y., Obayashi, M., Nakakuli, T. & the Deep Slab Project Group, 2009. Stagnant slab: a review, *Annu. Rev. Earth planet. Sci.,* **37,** 19–46.

Gilbert, H.J., Sheehan, A.F., Dueker, K.G. & Molnar, P., 2003. Receiver functions in the western United States, with implications for upper mantle structure and dynamics, *J. geophys. Res.,* **108**(B5), 2299, doi:10.1029/2001JB001194.

González-Fernández, A., Dañobeitia, J.J., Delgado-Argote, L.A., Michaud, F., Córdoba, D. & Bartolomé, R., 2005. Mode of extension and rifting history of upper Tiburón and upper Delfín basins, northern Gulf of California, *J. geophys. Res.,* **110,** B01313, doi:10.1029/2003JB002941.

Grand, S.P. & Helmberger, D.V., 1984. Upper mantle shear structure of North America, *Geophys. J. R. astr. Soc.,* **76,** 399–438.

Gu, Y., Dziewonski, A.M. & Agee, C.B., 1998. Global de-correlation of the topography of the transition zone discontinuities, *Earth planet. Sci. Lett.,* **157,** 57–67.

Gurrola, H. & Minster, J.B., 1998. Thickness estimates of the upper-mantle transition zone from bootstrapped velocity spectrum stacks of receiver functions, *Geophys. J. Int.,* **133,** 31–43.

Husebye, E.S., Chistoffersson, A. & Frasier, C.W., 1975. Orthogonal representations of array-recorded short period P-waves, *NATO ASI Series, Series E: Applied Sciences, no. 11, Exploitation of Seismograph Networks, Nordhoff,* Leiden, 297–309.

Inoue, T., Weidner, D.J., Northrup, P.A. & Parise, J.B., 1998. Elastic properties of hydrous ringwoodite (γ-phase) in Mg_2SiO_4, *Earth planet. Sci. Lett.,* **160,** 107–113.

Ito, E. & Takahasi, E., 1989. Postspinel transformations in the system Mg_2SiO_4-Fe_2SiO_4 and some geophysical implications, *J. geophys. Res.,* **94,** 10 637–10 646.

Jackson, I., 1983. Some geophysical constraints on the chemical composition of the Earth's lower mantle, *Earth planet. Sci. Lett.,* **62,** 143–164.

Jasbinsek, J.J., Dueker, K.G. & Hansen, S.M., 2010. Characterizing the 410 km discontinuity low-velocity layer beneath the LA RISTRA array in the North American Southwest, *Geochem. Geophys. Geosyst.,* **11,** Q03008, doi:10.1029/2009GC002836.

Kanasewich, E.R., 1973. *Time Sequence Analysis in Geophysics,* The University of Alberta Press, Edmonton, Canada, 364 pp.

Kennett, B., 1991. Seismic velocity gradients in the upper mantle, *Geophys. Res. Lett.,* **18,** 115–118.

Kennett, B. & Engdahl, E.R., 1991. Travel times for global earthquake location and phase identification, *Geophys. J. Int.,* **105,** 429–465.

Lebedev, S., Chevrot, S. & van der Hilst, R.D., 2002. The 660-km discontinuity within the subducting NW-Pacific lithospheric slab, *Earth planet. Sci. Lett.,* **205,** 25–35.

Li, C., van der Hilst, R.D., Engdahl, E.R. & Burdickm, S., 2008. A new global model for P wave speed variations in Earth's mantle, *Geochem. Geophys. Geosyst.,* **9,** Q05018, doi:10.1029/2007GC001806.

Ligorría, J.P. & Ammon, C.J., 1999. Iterative deconvolution and receiver-function estimation, *Bull. seism. Soc. Am.,* **89,** 1395–1400.

Litasov, K., Ohtani, E., Sano, A., Suzuki, A. & Funakoshi, K., 2005. In situ X-ray diffraction study of post-spinel transformation in a peridotite mantle: implication for the 660-km discontinuity, *Earth planet. Sci. Lett.,* **238,** 311–328.

Lizarralde, D. *et al.*, 2007. Variation in styles of rifting in the Gulf of California, *Nature,* **448,** 466–469.

Lonsdale, P., 1989. Geology and tectonic history of the Gulf of California, in *The Eastern Pacific Ocean and Hawaii, The Geology of North America,* Vol. **N,** pp. 499–521, eds Hussong, D., Winterer, E.I. & Decker, R.W., Geological Society of America, Boulder, Colorado.

Lonsdale, P., 1991. Structural patterns of the Pacific floor offshore of peninsular California, in *The Gulf and Peninsular Province of the Californias,* Vol. 47, pp. 87–125, eds Dauphin, J.P. & Simoneit, B.R.T., AAPG Memoir, Tulsa, OK, USA.

Mammericks, J. & Klitgord, K.D., 1982. Northern East Pacific rise: evolution from 25 m.y. B. P. to the present, *J. geophys. Res.,* **87,** 6751–6759.

McCroy, P.A., Wilson, D.S. & Stanley, R.G., 2009. Continuing evolution of the Pacific-Juan de Fuca-North America slab window system—a trench-ridge-transform example from the Pacific Rim, *Tectonophysics,* **464,** 30–42.

Menard, H.W., 1978. Fragmentation of the Farallon plate by pivoting subduction, *J. Geol.,* **86,** 99–110.

Michaud, E. *et al.*, 2006. Oceanic ridge subduction vs. slab break-off: plate tectonic evolution along the Baja California Sur continental margin since 15 Ma, *Geology,* **34,** 13–16.

Nagy, E.A. & Stock, J.M., 2000. Structural controls on the continent-ocean transition in the northern Gulf of California, *J. geophys. Res.,* **105**(B7), 16 251–16 269.

Oskin, M. & Stock, J., 2003. Miocene to Recent Pacific–North America plate motion and opening of the Upper Delfín Basin, northern Gulf of California, Mexico, *Bull. geol. Soc. Am.,* **115,** 1173–1190.

Owens, T.J., Nyblade, A.A., Gurrola, H. & Langston, C.A., 2000. Mantle transition zone structure beneath Tanzania, East Africa, *Geophys. Res. Lett.,* **27,** 827–830.

Persaud, P., Pérez-Campos, X. & Clayton, R., 2007. Crustal thickness variations in the margins of the Gulf of California from receiver functions, *Geophys. J. Int.,* **170,** 687–690.

Ravenaugh, J. & Sipkin, S.A., 1994. Seismic evidence for silicate melt atop the 410-km mantle discontinuity, *Nature,* **369,** 474–476.

Ringwood, A.E., 1970. Phase transformations and the constitution of the mantle, *Phys. Earth planet. Inter.,* **3,** 109–155.

Savage, B., 2012. Seismic constraints on the water flux delivered to the deep Earth by subduction, *Geology,* **40,** 232–238.

Schmandt, B., Dueker, K.G., Hansen, S.M., Jasbinsek, J.J. & Zhang, Z., 2011. A sporadic low-velocity layer atop the western U.S. mantle transition zone and short-wavelength variations in transition zone discontinuities, *Geochem. Geophys. Geosyst.,* **12,** Q08014, doi:10.1029/2011GC003668.

Shearer, P.M., 1990. Seismic imaging of upper-mantle structure with new evidence for a 502-km discontinuity, *Nature,* **344,** 121–126.

Simmons, N.A. & Gurrola, H., 2000. Multiple seismic discontinuities near the base for the transition zone in the Earth's mantle, *Nature,* **405,** 559–562.

Sinogeikin, S.V., Bass, J.D. & Katsura, T., 2003. Single-crystal elasticity of ringwoodite to high pressures and high temperatures: implications for 520 km seismic discontinuity, *Phys. Earth planet. Inter.,* **136,** 41–66.

Smyth, J.R. & Frost, D.J., 2002. The effect of water on the 410-km discontinuity: an experimental study, *Geophys. Res. Lett.,* **29**(10), 1485, doi:10.1029/2001GL014418.

Song, T.-R.A., Helmberger, D.V. & Grand, S.P., 2004. Low-velocity zone atop the 410-km seismic discontinuity in the northwestern United States, *Nature,* **427,** 530–533.

Stammler, K., Kind, R., Petersen, N., Korasev, G., Vinnik, L. & Qiyuan, L., 1992. The upper mantle discontinuities: correlated or anticorrelated? *Geophys. Res. Lett.,* **19**(15), 1563–1566.

Vacher, P., Mocquet, A. & Sotin, C., 1998. Computation of seismic profiles from mineral physics: the importance of the non-olivine components for explaining the 660 km depth discontinuity, *Phys. Earth planet. Inter.,* **106,** 275–298.

van der Mijde, M., Marone, F., Giardini, D. & van der Lee, S., 2003. Seismic evidence for water deep in Earth's upper mantle, *Science,* **300,** 1556–1558

Vinnik, L.P., 1977. Detection of waves converted from P to SV in the mantle, *Phys. Earth planet. Inter.,* **15,** 39–45.

Vinnik, L.P. & Farra, V., 2007. Low S velocity atop the 410-km discontinuity and mantle plumes, *Earth planet Sci. Lett.,* **262,** 398–412.

Wang, Y., Forsyth, D.W. & Savage, B., 2009. Convective upwelling in the mantle beneath the Gulf of California, *Nature,* **462,** 499–501.

Wessel, P. & Smith, W.H.F., 1991. Free software helps map and display data, *EOS, Trans. Am. geophys. Un.,* **72**(441), 445–446.

Yuen, D.A., Reuteler, D.M., Balachandar, S., Steinbach, V., Malevsky, A.V. & Smedsmo, J.J., 1994. Various influences on three-dimensional mantle convection with phase transitions, *Phys. Earth planet. Inter.,* **86,** 185–203.

Zhang, X., Paulssen, H., Lebedev, S. & Meier, T., 2009. 3D shear velocity structure beneath the Gulf of California from Rayleigh wave dispersion, *Earth planet. Sci. Lett.,* **279,** 255–262.

Zhao, D., Xu, Y., Wiens, D.A., Dorman, L, Hilderbrand, J. & Webb, S., 1997. Depth extent of the Lau Back-Arc Spreading Center and its relation to subduction processes, *Science,* **278,** 254–257.

SUPPORTING INFORMATION

Additional Supporting Information may be found in the online version of this paper:

Figure S1. (a) Station locations and pierce points for the 410 (red crosses) and the 660 (green crosses) discontinuities. Triangles denote NARS-Baja stations; inverted triangles, RESBAN stations; squares, SSN stations and circles, SCSN stations. The black dots correspond to the $0.5^\circ \times 0.5^\circ$ grid nodes. Profile AA′ is shown in Fig. S3. Thick black arrows indicate the current Pacific (PAC)–North America (NAM) relative plate motion direction N37°W (Atwater & Stock 1998). RIV, Rivera Plate. (b) Number of RFs obtained at each station. The stations are grouped by network.

Figure S2. Upper-mantle discontinuities using iasp91 (a–c) and TNA (d–f) models as reference. Both include RFs from 16 stations of the Southern California Seismic Network (SCSN). (a) and (f) Number of RFs per node for the 410 (top) and the 660 (bottom). The minimum allowed for the stacking was 10. (b) and (d) Complexity of the RFs for the 410 (top) and the 660 (bottom). The colour corresponds to the NPV for the mean RF at each node; blue colours denote a single pulse, while warm colours denote multiple pulses. (c) and (d) Topography of the 410 (top) and the 660 (centre). The colour corresponds to the depth with respect to 428 and 383 km average depth for the 410 for iasp91 (c) and TNA (d), respectively; and 676 and 660 km for the 660 for iasp91 (c) and TNA (d), respectively. 'T' denotes a hill in the 410, described on the text. The bottom panel shows the transition zone thickness (TZT), colour corresponds to the variation with respect to average of 248 and 278 km for iasp91 (c) and TNA (d), respectively. General features observed at the 410 and the 660 are similar using both reference models and similar within the Gulf without using the data from SCSN stations (Fig. 3).

Figure S3. Profile along and crossing the Gulf of California. Top: Surface provinces in the region of the study and location of profile A–A′ (black line). Data from SCSN are included; the results along the Gulf are similar to those without including these stations. The grey areas correspond to the remains of the Guadalupe (Gua) and Magdalena (Mag) plates. T-A FZ, Tosco-Abreajos fault zone; EPR, East Pacific Rise; GEP, Gulf Extension Province. Bottom: RFs within 50 km from each profile, superimposed to tomography from Li *et al.* (2008). Colours on top of the profile correspond to the Gulf region: brown, rifting; blue, oceanic crust; pink, transition region (http://gji.oxfordjournals.org/lookup/suppl/doi:10.1093/gji/ggt133/-/DC1).

Please note: Oxford University Press are not responsible for the content or functionality of any supporting materials supplied by the authors. Any queries (other than missing material) should be directed to the corresponding author for the paper.